TanDEM-X Performance Optimization

S. Huber* H. Fiedler G. Krieger M. Zink

German Aerospace Center (DLR)
Microwaves and Radar Institute - Oberpfaffenhofen
Münchner Str. 20, 82234 Weßling, Germany
Fax: +49 (0)8153 28 1449

Abstract

TanDEM-X, **T***erraSAR-X* **a***dd-o***n** *for* **D***igital* **E***levation* **M***easurement, is a space borne Earth remote sensing mission with the goal of generating a global Digital Elevation Model with an unprecedented accuracy, corresponding to the HRTI-3 specifications. TanDEM-X will orbit in a special HELIX formation, with the fully compatible TerraSAR-X satellite in order to collect interferometric SAR data. It is planned to image the Earth's surface twice with different baselines. Presented in this paper is an optimization strategy, with the objective of a quasi-homogeneous height accuracy, which meets the HRTI-3 standard. The optimization has a major impact on the data acquisition plan.*

1 Introduction

For TanDEM-X [3], the acquisition of a Digital Elevation Model (DEM) on a global scale requires an optimized mission plan, since the time, where both satellites are in orbit simultaneously, is limited to three years. Within this time the landmass is imaged in strip map mode twice, with two different heights of ambiguity, which allows for multi baseline phase unwrapping techniques. Due to the 167 satellite orbits, the region to be imaged has an across-track extension of about 240 km, at the equator. This region is subdivided into several swaths. The swath-width is determined by the timing, but also by the pattern of the SAR antenna. The shape of the antenna beam and SAR system parameters, like the pulse repetition frequency (PRF), are in the focus of the optimization. The most important parameter of a DEM is the height accuracy. Therefore, the optimization concentrates directly on this quantity, rather than trying to maximize a single parameter, e.g. the signal to noise ratio (SNR). The vertical accuracy requirements are summarised in Table 1. The terrain slope is denoted by α.

Requirement	**Spec.**	**HRTI-3**
absolute vertical accuracy (global)	90 % linear error	10 m
relative vertical accuracy $1° \times 1°$ cell	90 % linear point-to-point error	2 m, $\lvert\alpha\rvert \leq 20\,\%$ 4 m, $\lvert\alpha\rvert > 20\,\%$

Tab. 1: TanDEM-X DEM specifications

In the first part of the paper, the height performance model is presented. Based on this model, the optimization strategy is described in the next chapter. In the last part, a method for combining multiple interferometric acquisitions is derived.

2 Performance Model

The principle of SAR interferometry is to utilize the phase difference between two coregistered SAR images. After phase unwrapping and geocoding the phase difference is transformed into terrain height with respect to a reference Earth-model, here WGS84. A measure of the quality of an interferogram is the correlation coefficient or coherence [5]. Given the complex valued SAR images u_1 and u_2 the correlation coefficient is defined as

$$\gamma = \frac{\mathrm{E}\{u_1 u_2^*\}}{\sqrt{\mathrm{E}\{u_1 u_1^*\}\mathrm{E}\{u_2 u_2^*\}}} \quad . \tag{1}$$

Assuming error sources, which can be modelled as uncorrelated, additive random processes, the total coherence equates

$$\gamma = \gamma_{SNR} \cdot \gamma_{AASR} \cdot \gamma_{RASR} \cdot \gamma_{\mathrm{rg}} \cdot \gamma_{\mathrm{az}} \cdot \gamma_{\mathrm{vol}} \cdot \gamma_{\mathrm{temp}} \quad . \tag{2}$$

The single contributions are:

*sigurd.huber@dlr.de

γ_{SNR}	decorrelation due to thermal receiver noise and quantization
γ_{AASR}	azimuth ambiguity coherence
γ_{RASR}	range ambiguity coherence
γ_{rg}	range-coregistration and baseline decorelation
γ_{az}	losses from azimuth-coregistration and doppler shift
γ_{vol}	volume decorrelation
γ_{temp}	temporal decorrelation

The coherence caused by receiver noise and quantization errors is combined in a single expression, since the block adaptive quantizer (BAQ) is a nonlinear device. In particular the output signal to noise ratio (SNR) of the BAQ depends on the input SNR of the BAQ. In principle also the ambiguous signals pass the BAQ and are transformed in a nonlinear way, but compared to the receiver noise power, the ambiguous signal power is small. Therefore, the coherence due to ambiguities can be treated in a separate term.
Utilizing equation (1) yields for the coherence, resulting from thermal receiver noise,

$$\gamma_{SNR} = \frac{1}{\sqrt{\left(1+SNR_1^{-1}\right)\left(1+SNR_2^{-1}\right)}} \quad . \tag{3}$$

The indices denote the two interferometric channels. Similar expressions can be found for the range- and azimuth correlation coefficients:

$$\gamma_{AASR} = \frac{1}{\sqrt{\left(1+AASR_1\right)\left(1+AASR_2\right)}} \quad , \tag{4}$$

and

$$\gamma_{RASR} = \frac{1}{\sqrt{\left(1+RASR_1\right)\left(1+RASR_2\right)}} \quad . \tag{5}$$

The fourth expression is related to the coherence loss caused by misregistration in range as well as baseline decorrelation. Because of the imaging geometry the ground range spectra are mutually shifted. Filtering the range spectra to a common frequency band compensates the effect of baseline decorrelation. For the remaining coherence, caused by misregistration in range, results then [2]

$$\gamma_{rg} = \mathrm{sinc}(\pi \partial r) \quad , \tag{6}$$

where ∂r denotes the relative range shift between the two SAR images in fractions of a resolution cell. Here unweighted processing of the rectangular range spectra is assumed. The azimuth coherence obeys two major effects: mutual shift of the Doppler spectra and coregistration errors in azimuth. The first effect is caused by an along track displacement of the two phase centers. Then the coherence can be calculated according to [2]

$$\gamma_{az} = \frac{\int H_1(f) H_2(f) \exp(-j2\pi\delta\tau_{az} f)\mathrm{d}f}{\sqrt{\int |H_1(f)|^2 \mathrm{d}f}\sqrt{\int |H_2(f)|^2 \mathrm{d}f}}, \tag{7}$$

with $\delta\tau_{az} = \delta az / v_{\mathrm{grd}}$ the coregistration error in azimuth. The transfer functions $H_1(f)$ and $H_2(f)$ are given as the product of the two-way antenna pattern with the envelope of the azimuth processing filter $H_{az}(f)$:

$$H_1(f) = G_{\mathrm{Tx}}(f) G_{\mathrm{Rx},1}(f) H_{az}(f) \quad , \tag{8}$$

$$H_2(f) = G_{\mathrm{Tx}}(f) G_{\mathrm{Rx},2}(f) H_{az}(f) \quad . \tag{9}$$

The index Tx denotes the transmitting satellite, while Rx,1 and Rx,2 indicate the first and the second satellite receiving, respectively.
Another error source results from volumetric scattering, which occurs mainly in vegetated areas. Assuming a vertical scattering model which fades exponentially,

$$\sigma_0(z) = \exp\left(-2\beta \frac{h_{\mathrm{v}} - z}{\cos(\theta_{\mathrm{i}})}\right), 0 \le z < h_{\mathrm{v}}, \tag{10}$$

the coherence can be computed as [2]

$$\gamma_{\mathrm{vol}} = \frac{\int \sigma_0(z) \exp(j2\pi z / h_{\mathrm{amb}})\mathrm{d}z}{\int \sigma_0(z)\mathrm{d}z} \quad , \tag{11}$$

where h_{v} is the volume height, h_{amb} denotes the height of ambiguity, β the extinction and θ_{i} is the incident angle.
The last coherence term describes decorrelation as result of change in the scene during the acquisition of the two interferometric channels. In the this model, temporal decorrelation is neglected. However, this effect might become significant, especially for vegetated areas and for large along track baselines.
Given the correlation γ of the two SAR images, the distribution of the interferometric phase errors is described by the probability density function (pdf) [1]

$$p_\phi(\phi) = \frac{\Gamma(N+0.5)(1-|\gamma|^2)^N |\gamma| \cos\phi}{2\sqrt{\pi}\Gamma(N)(1-|\gamma|^2\cos^2\phi)^{N+0.5}} + \frac{(1-|\gamma|^2)^N}{2\pi} {}_2F_1(N,1;0.5;|\gamma|^2\cos^2\phi) \quad . \tag{12}$$

Here Γ denotes the gamma function, ${}_2F_1$ is the Gauss hypergeometric function, N is the effective number of looks and Φ the interferometric phase error. The 90 % point-to-point error is defined via the integral over the difference *pdf* of two phase errors in a $1^\circ \times 1^\circ$ cell, which corresponds approximately to a $(100 \times 100)\,\mathrm{km}^2$ square. Therefore, the joint *pdf*, which is given by the convolution of the single phase error *pdf*s, has to be evaluated:

$$\int_{-\phi_{90\%}}^{\phi_{90\%}} p_\phi(\phi) * p_\phi(\phi)\mathrm{d}\phi = 0.9 \quad . \tag{13}$$

Figure 1 shows the 90 % phase error as function of the coherence for different number of looks, after unwrapping. In case of zero coherence the phase errors are distributed uniformly and the 90 % phase error equates

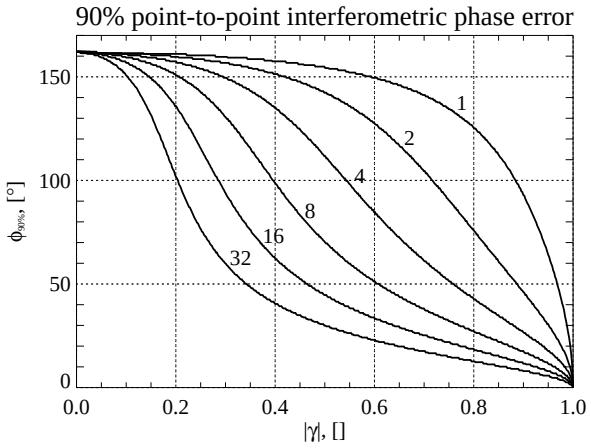

Fig. 1: 90 % point-to-point interferometric phase errors as function of the coherence, with the numbers above the curves indicating the number of looks

$0.9 \cdot 180\,^\circ = 162\,^\circ$. For coherence equal one, no phase errors are present. The relative height error is then derived by scaling the interferometric phase error with the height of ambiguity:

$$h_{90\%} = h_{\mathrm{amb}} \frac{\phi_{90\%}}{2\pi} \quad , \tag{14}$$

where the height of ambiguity is given as

$$h_{\mathrm{amb}} = \frac{\lambda r \sin\theta_{\mathrm{i}}}{b_{\perp}} \quad , \tag{15}$$

depending on the slant range r, the transmitted wavelength λ and the orthogonal baseline $b_{\perp}$. This performance model forms the basis of the performance optimization.

3 Performance Optimization

The goal of the performance optimization is to achieve a quasi homogenous height accuracy. In order to apply multi baseline phase unwrapping techniques, the Earth surface is imaged twice. The two acquisitions will be shifted against each other half a swath width (≈ 15 km) in ground range direction. The optimization shall give information about how many beams have to be used in order to meet the performance requirements, about the position and the shape of the beams and also about the expected data rates for each swath.
The flowchart in figure 2 shows the tasks involved in the performance optimization. Due to the complexity and high number of parameters, the optimization is segmented into several blocks, each focusing on a couple of parameters. Concerning the beam optimization it showed, that without tapering of the antenna pattern, the best tradeoff between beamwidth and SNR is achieved. As a result, the area of 240 km can best be

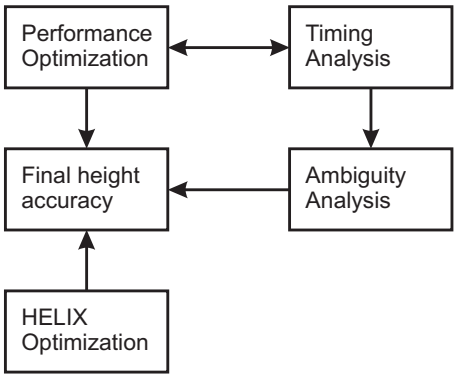

Fig. 2: performance optimization

covered with nine beams. Also more beams are possible, but in this case the mission time sets a stringent constraint. The overlap between adjacent swaths is 4 km, which is sufficient to ensure bundle adjustment techniques. Figure 3 depicts the optimization result for fixed heights of ambiguities. As can be seen, the intersection-points of adjacent beams lie on a constant height.

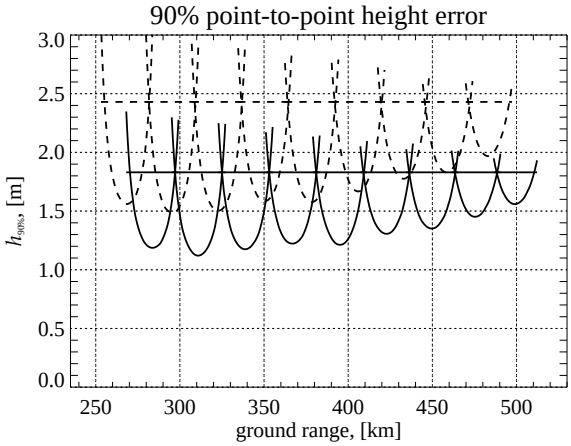

Fig. 3: optimized height performance for fixed heights of ambiguities: 30 m (solid) and 40 m (dashed)

The results of the beam optimization are validated with the timing analysis. Here valid PRFs are calculated, taking into account nadir ambiguities and delayed echo returns. Another result from the timing analysis is the expected data rate, which is calculated according to

$$R_{\mathrm{BAQ8:}x} = 2 \cdot \mathrm{E}\{EWL\} \cdot f_{\mathrm{s}} \cdot x \cdot PRF \quad , \tag{16}$$

where EWL is the echo-window-length, $f_{\mathrm{s}} = 110$ MHz the sampling frequency and x the quantization and PRF the pulse-repetition-frequency. The factor 2 accounts for in-phase- and quadrature-channel. The expected data rates are well below 500 MBit/s (BAQ8:3) for every satellite.

A secondary optimization goal arises from azimuth- and range-ambiguities, which define a lower and an upper bound for the pulse repetition frequencies, respectively. The limit for the ambiguities is chosen to be $-17\,\mathrm{dB}$. This requires the PRFs to be in the interval between 3050 Hz and 4000 Hz.
In a separate procedure the HELIX parameters are optimized, such that the height of ambiguity is as close as possible to a fixed value. With this the final height accuracy can be calculated. In figure 4 the effect of the varying height of ambiguity can be observed. Here three sets of different HELIX parameters were used.

4 Fusion of Interferograms

Since the Earth surface is imaged twice, this offers the opportunity to fuse the interferograms into one, resulting in a further improved height accuracy. Especially in overlapping regions of adjacent swaths the effect of the low antenna gain can be compensated.
Having N height measurements disturbed by errors with unequal variances Δh_i^2, the equation for the combined height error variance can be formulated as

$$\Delta h_{\mathrm{comb}}^2 = \frac{\sum_{i=1}^{N} w_i^2 \Delta h_i^2}{\left(\sum_{i=1}^{N} w_i\right)^2} \quad . \tag{17}$$

In order to minimize this expression, the partial derivatives with respect to the real valued weights w_i are taken

$$\frac{\partial \Delta h_{\mathrm{comb}}^2}{\partial w_i} = \frac{w_i \Delta h_i^2 \sum_{i=1}^{N} w_i - \sum_{i=1}^{N} w_i^2 \Delta h_i^2}{0.5\left(\sum_{i=1}^{N} w_i\right)^3} \quad . \tag{18}$$

The solution of this system of equations is

$$w_i = \frac{\Delta h_i^{-2}}{\sum_{k=1}^{N} \Delta h_k^{-2}} \quad . \tag{19}$$

These weights can for example be derived from coherence maps of the corresponding interferometric SAR images. Inserting this result into equation (17) yields for the final error in the combined height estimate

$$\Delta h_{\mathrm{comb}}^2 = \frac{1}{\sum_{i=1}^{N} \Delta h_i^{-2}} \quad . \tag{20}$$

Figure 4 shows in the upper plot the height errors for the two acquisitions (solid and dashed). The combination of the measurements is depicted in the lower plot. Here the improvement of the height accuracy becomes evident, especially in the overlap regions of adjacent swaths. The variation of the height error is in the order of 0.5 m and can be, compared to the error plot in the upper image, considered as quasi-homogeneous.
The previous plots show optimization results for the equator region. The optimization of the performance can be extended to a second dimension, which is the latitude. This is a necessary step, since the satellite formation or the orbit height changes over latitude, which has an impact on the height of ambiguity, the swath width and position and thus, on the overall height performance. Image 5 shows the estimated height error for flat terrain for a soil and rock backscatter model [4], using both, the small and large baseline HELIX configurations. Figure 6 depicts the height accuracy for a terrain slope of 20 % facing away from the radar. Here the effect of reduced SNR, due to lower backscatter, becomes evident. For steeper terrain, as it is the case in mountainous regions, further interferometric acquisitions are necessary. In the last picture (7) the height accuracy in the presence of volume decorrelation is shown. The tree height is 20 m and the extinction $\beta = 1\,\mathrm{dB/m}$. Here the performance requirement is violated in small regions, but it is expected, that the 2 m point-to-point requirement for 90 % of the global landmass can be achieved.

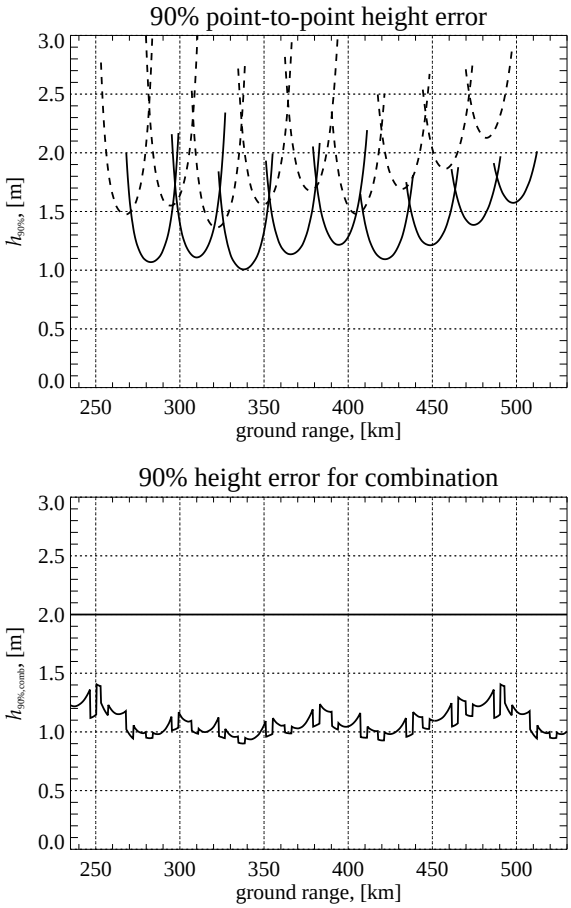

Fig. 4: 90 % height error for large height of ambiguity (dashed) and for small height of ambiguity (solid) (upper plot); combination of height errors (lower plot)

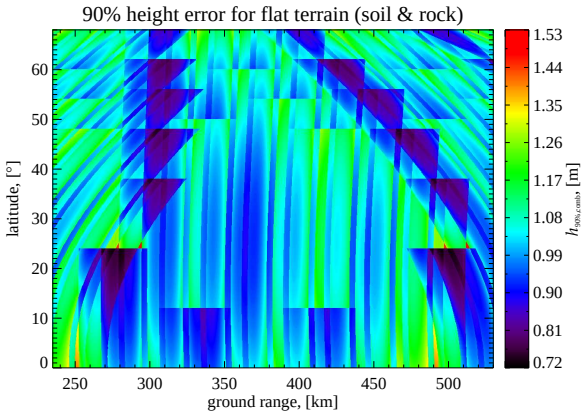

Fig. 5: Predicted point-to-point 90 % height accuracy for soil and rock surfaces in case of flat terrain after the optimum combination of all data from both the small and large baseline HELIX configurations

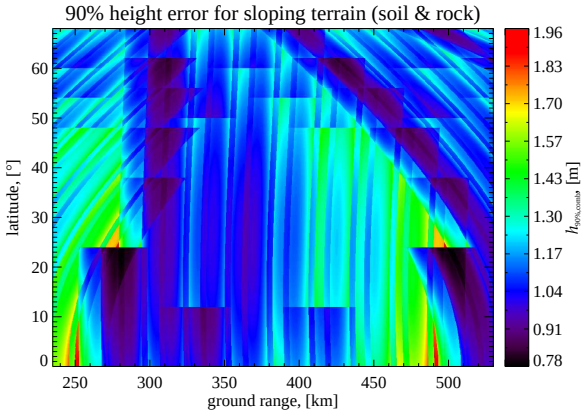

Fig. 6: Predicted point-to-point 90 % height accuracy for soil and rock surfaces in case of slopes of 20 % facing away from the radar after the optimum combination of all data from both the small and large baseline HELIX configurations

5 Conclusions and Future Work

Based on a refined performance model a method has been established to optimize the height accuracy with the objective of a quasi-homogeneous performance. A further improvement can be achieved by combining several interferometric height measurements. In this case the approach of weighted least squares was utilized.

Concerning future work, the performance model will be further extended, especially in view of the errors introduced by the BAQ. In regions with inhomogeneous reflectivity distribution, phase errors due to BAQ mismatch are expected. The performance shall be computed on a global scale, incorporating backscatter maps derived from other SAR missions, like TerraSAR-X.

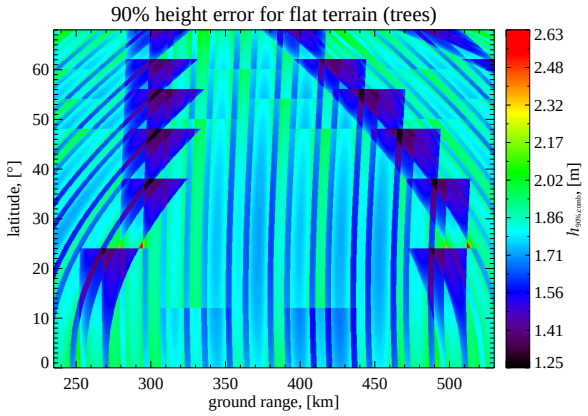

Fig. 7: Predicted point-to-point 90 % height accuracy for trees after optimum combination of all data from both the small and large baseline HELIX configurations. This analysis is based on a tree height of 20 m and an extinction of 1 dB/m

6 Acknowledgement

The TanDEM-X project is partly funded by the German Federal Ministry of Economics and Technology (Förderkennzeichen 50 EE 0601).

References

[1] R. Bamler and P. Hartl. Synthetic aperture radar interferomerty. Technical report, German Aerospace Center (DLR), 1998.

[2] Gerhard Krieger, Alberto Moreira, Irena Hajnsek, Marian Werner, Marwan Younis, and Manfred Zink. TanDEM-X: A Satellite Formation for High Resolution SAR Interferometry. *IEEE Transactions on Geoscience and Remote Sensing*, 2007 - in print.

[3] Gerhard Krieger, Alberto Moreira, David Hounam, Marian Werner, Sebastian Riegger, and Eckard Settelmeyer. A Tandem TerraSAR-X Configuration for Single-Pass SAR Interferometry. *Proceedings of the International Conference on Radar Systems*, 2004.

[4] F. T. Ulaby and M. C. Dobson. *Handbook of Radar Scattering Statistics for Terrain.* Artech House, Inc., 1989.

[5] Howard A. Zebker and John Villasenor. Decorrelation in Interferometric Radar Echos. *IEEE Transactions on Geoscience and Remote Sensing*, 30(5):950–959, September 1992.